Synthesis, Spectroscopy, and Structural Characterization of Six-Coordinate Bis(aryldiazenido)rhenium and Bis(diarylhydrazido)rhenium Complexes. X-ray Structures of $(Et_4N)[Re(NNPh)_2(O_2C_6H_4)_2]$, $(Et_4N)[Re(NNPh_2)_2(O_2C_6H_4)_2]$, and $Na[Re(NNPh)_2(O_2C_6H_4)_2]\cdot CH_3CN$

Peter B. Kettler, Yuan-Da Chang, and Jon Zubieta*

Department of Chemistry, Syracuse University, Syracuse, New York 13244

Received March 16, 1994[⊗]

The reactions of the *cis*-dioxorhenium(VII)−catecholate complex $[(CH_3CH_2)_4N][ReO_2(O_2C_6H_4)_2]$ (**1**) with either monosubstituted organohydrazines ($C_6H_5NHNH_2$; 4-$BrC_6H_4NHNH_2$) or 1,1-disubstituted organohydrazines (Ph_2NNH_2) yield the *cis*-bis(diazenido) core complexes $[(CH_3CH_2)_4N][Re(NNR)_2(O_2C_6H_4)_2]$ (**5**, R = C_6H_5; **6**, R = 4-BrC_6H_4) and the *cis*-bis(hydrazido) core species $[(CH_3CH_2)_4N][Re(NNPh_2)_2(O_2C36H_4)_2]$ (**7**). Elution of **5** in a 3:1 mixture of toluene/methanol on a column of silica gel resulted in cation exchange to give $Na[Re(NNPh)_2(O_2C_6H_4)_2]\cdot CH_3CN$ (**8**) as a one-dimensional polymer $\{[Na(CH_3CN)]^+[Re(NNPh)_2(O_2C_6H_4)_2]^-\}_2$. Crystal data for $C_{32}H_{38}N_5O_4Re$ (**5**): $P2_1/c$, a = 14.458(3) Å, b = 10.436(2) Å, c = 21.767(4) Å, β = 107.04(3)°, V = 3140(2) Å^3, Z = 4, D_{calc} = 1.572 g cm^{-3}; structure solution and refinement based on 3256 reflections with $I_o \geq 3\sigma(I_o)$ converged at R = 0.053. Crystal data for $C_{44}H_{48}N_5O_4Re$ (**7**): $P\bar{1}$, a = 11.660(2) Å, b = 11.864(2) Å, c = 15.400(2) Å, α = 107.12(3)°, β = 94.99(3)°, γ = 97.61(3)°, V = 2000(1) Å^3, Z = 2, D_{calc} = 1.490 g cm^{-3}; 3702 reflections, R = 0.0534. Crystal data for $C_{26}H_{18}N_5NaO_4Re$ (**8**): $P2/n$, a = 5.785(1) Å, b = 9.670)2) Å, c = 23.142(5) Å, β = 90.91(3)°, V = 1294.4(7) Å^3, Z = 2, D_{calc} = 1.737 g cm^{-3}; 1517 reflections, R = 0.049.

Introduction

The use of the radionuclide technetium-99m is ubiquitous in diagnostic nuclear medicine. This radionuclide has several distinct advantages over other radionuclides used in diagnostic nuclear medicine including cost, availability, low radiation absorbed dose, and the ability to render results for clinical evaluation very quickly. These advantages are in part manifested by the nuclear properties of the meta-stable isotope ($t_{1/2}$ = 6 h; γ = 140 keV). Technetium-99m imaging agents have been developed that are highly successful in imaging vital organs such as the heart, brain, lungs, GI tract, and kidneys.[1−5]

More recently, radiopharmaceuticals utilizing rhenium, the third-row congener of technetium, with its corresponding radioisotopes rhenium-186 and rhenium-188 are being developed.[6−10] The nuclear properties of Re-186 ($t_{1/2}$ = 90 h; γ = 137 keV; β = 1.07 MeV) enable the isotope to be imaged by γ-cameras utilized in conventional ^{99m}Tc diagnostic imaging. Also, the energy of the β-emission enables it to be utilized as a therapeutic radiopharmaceutical. A rhenium radiopharmaceutical, ^{186}Re(Sn)HEDP has been developed for the palliation of painful osseous metastases.[10,11]

One approach is targeting radiopharmaceutical delivery systems exploits what is termed the "metal-tagged" approach.[5,12] Specifically, the covalent attachment of a radionuclide to an antibody by a bifunctional chelate has been utilized for diagnostic oncological applications and also to image focal sites of infection.[13]

Recently, we have explored the coordination chemistry of technetium organohydrazine complexes[14−18] to model the uptake of ^{99m}Tc by a bifunctional hydrazine reagent. Technetium(V)

[⊗] Abstract published in *Advance ACS Abstracts,* November 15, 1994.

(1) Pinkerton, T. C.; Desilets, C. P.; Hoch, D. J.; Mikelsons, M. V.; Wilson, G. M. *J. Chem. Ed.* **1985**, 462, 965.
(2) Clarke, M. J.; Podbielski, L. *Coord. Chem. Rev.* **1987**, *78*, 253.
(3) Steigman, J.; Echelman, W. C. *The Chemistry of Technetium in Medicine*; Nuclar Science Publications NAS-NS-307; National Academy Press: Washington, DC, 1992.
(4) Deutsch, E.; Libson, K.; Jurisson, S.; Lindoy, L. F. *Progr. Inorg. Chem.* **1983**, *30*, 75.
(5) Jurisson, S.; Bering, D.; Jia, W.; Ma, D. *Chem. Rev.* **1993**, *93*, 1173.
(6) Deutsch, E.; Libson, K.; Vanderheyden, J.-L.; Ketring, A. R.; Maxon, H. P. *Nucl. Med. Biol.* **1986**, *13*, 465.
(7) Ehrhardt, J.; Ketring, A. R.; Turpin, T. A.; Razavi, M.-S.; Vanderheyden, J.-L.; Su, F.-M.; Fritzberg, A. R. In *Tetchnetium and Rhenium in Chemistry and Nuclear Medicine 3*; Nicollini, M., Bandoli, G., Mazzi, U., Eds.; Castina International: Verona, 1990; pp 631−634.
(8) Häfeli, U.; Tiefenance, L.; Schuberger, P. A. In *Tetchnetium and Rhenium in Chemistry and Nuclear Medicine 3*; Nicollini, M., Bandoli, G., Mazzi, U., Eds.; Castina International: Verona, 1990; pp 643−646.
(9) Nosco, D. L.; Tofe, A. J.; Dunn, T. J.; Lyle, L. R.; Wolfangel, R. G.; Bushman, M. J.; Grummon, G. D.; Helling, D. E.; Marmion, M. E.; Miller, K. M.; Pipes, D. W.; Strubel, T. W.; Wester, D. W. In *Technetium and Rhenium in Chemistry and Nuclear Medicine 3*; Nicollini, M., Bandoli, G., Mazzi, U., Eds.; Castina International: Verona, 1990; pp 381−392.
(10) Maxon, H. R., III; Schroder, L. E.; Thomas, S. R.; Hertzberg, V. S.; Deutsch, E.; Samotunga, R. C.; Libson, K.; Williams, C. C.; Maulton, J. S.; Schneider, H. J. In *Technetium and Rhenium in Chemistry and Nuclear Medicine 3*; Niccolini, M., Bandoli, G., Mazzi, U., Eds.; Castina International: Verona, 1990; pp 733−9.
(11) Vanderheyden, J.-L.; Heeg, M. J.; Deutsch, E. *Inorg. Chem.* **1988**, *24*, 1666.
(12) Meares, C. F. In *Protein Tailoring for Food and Medical Uses*; Feeney, R. E., Whiteker, J. R., Eds.; Marcel Dekker: New York, 1986; p 339. Yeh, S. M.; Sherman, D. G.; Meares, C. F. *Anal. Chem.* **1979**, *100*, 152. Meares, C. F.; Wensel, T. G. *Acc. Chem. Res.* **1984**, *17*, 202. Brechbiel, M. W.; Gansow, O. A.; Atcher, R. W.; Schlom, J.; Esteban, J.; Simpson, D. E.; Colcher, D. *Inorg. Chem.* **1986**, *25*, 2772 and references therein.
(13) For the specific case of 99m-Tc labeling, see: Lanteigne, D. D.; Hnatowich, J. *Int. J. Appl. Radiat. Isot.* **1984**, *35*, 617. Arano, Y.; Yokoyama, A.; Furukawa, T.; Horiuchi, K.; Yahata, T.; Saji, H.; Sakahara, H.; Nakashima, T.; Koizumi, M.; Endo, K.; Torizuka, K. *J. Nucl. Chem.* **1987**, *28*, 1027. Fritzberg, A.; Kasina, S.; Vanderheyden, J. L.; Srinivasan, A. Eur. Patent Appl. Ep. 284071, 1988. Liang, F. H.; Virzi, F.; Hnatowich, D. J. *Nucl. Med.* 4Biol. **1987**, *14*, 63. Lever, S. Z.; Baidov, K. E.; Kramer, A. V.; Burns, H. D. *Tetrahedron Lett.* **1988**, *29*, 3219. Eary, J. F.; Schroff, R. F.; Abrams, P. G.; Fritzberg, A. R.; Morgan, A. C.; Kasina, S.; Reno, J. M.; Srinivasan, A.; Woodhouse, C. S.; Wilbur, D. S.; Natale, R. B.; Collins, C.; Stehlin, J. S.; Mitchell, M.; Nelp, W. B. *J. Nucl. Med.* **1989**, *30*, 25.
(14) Abrams, M. J.; Shaikh, S. N.; Zubieta, J. *Inorg. Chim. Acta* **1990**, *173*, 133.

0020-1669/94/1333-5864$04.50/0

oxo precursors were found to add readily under mild conditions to hydrazinopyridine-modified proteins to yield stable ^{99m}Tc-labeled proteins in >90% radiometric yield.[19] ^{99m}Tc–hydrazinopyridine–polyclonal IgG conjugates have been demonstrated to be useful agents for the imaging of focal sites of infection.[20]

Since the coordination chemistry of technetium oxo catecholates, which serves as a model for $[TcO(glucoheptonate)_2]^-$, a common synthetic precursor in the preparation of ^{99m}Tc protein conjugates with organohydrazines, has been explored, we deemed it necessary to examine the reactions of the analogous rhenium oxo catecholates with organohydrazines due to the utility of the $^{186/188}$Re radionuclides in therapeutic radiopharmaceuticals.

As we have reported previously, the reactions of Re(V) oxo catecholate complexes with organohydrazines lead only to the isolation of intractable solids.[21] However, the reaction of the previously reported[22,23] *cishdioxorhenium*(VII)–catecholate complex $[(CH_3CH_2)_4N]^+[ReO_2(cat)_2]^-$ (**1**) with either monosubstituted organohydrazines ($C_6H_5NHNH_2$; 4-Br-$C_6H_4NHNH_2$) or 1,1-disubstituted organohydrazines ($(C_6H_5)_2NNH_2$) led to the formation of the *cis* bis(diazenido) complexes $[(CH_3CH_2)_4N]^+[Re(N_2R)_2(cat)_2]^-$ (**5**, R = C_6H_5; **6**, R = 4-BrC_6H_4) and the *cis*-bishydrazido complex $[(CH_3CH_2)_4N]^+[Re(N_2R_1R_2)(cat)_2]^-$ (**7**, $R_1 = R_2 = C_6H_5$). These complexes were characterized by elemental analysis, IR, UV–visible, and NMR (^{1}H, ^{13}C) spectroscopy. In the case of **5** and **7**, the complexes were structurally characterized by X-ray crystallography. Also, a modification of the procedure to prepare previously reported *cis*-dioxorhenium(VII) catecholate complexes is reported along with the clarification of previously reported errors in the spectroscopic data.

Finally, an unusual cation exchange occurs when **5** is dissolved in a 3:1 mixture of toluene/methanol and eluted on a column of silica gel. The silica gel acts as a cation exchange support which exchanges the tetraethylammonium cation for a sodium cation to yield the sodium salt of **5**, $\{Na^+[Re(N_2(C_6H_5))_2(cat)_2]^-\}_\infty$ (**8**), as a one-dimensional polymer. This complex has been by characterized by spectroscopic and structural methods as described above. This complex has appreciable water solubility which has physiological implications toward the stability of the modeled bifunctional chelate *in vivo*.

Experimental Section

General Considerations. NMR spectra were recorded on a General Electric QE 300 (^{1}H, 300.10 MHz; ^{13}C, 75.47 MHz) spectrometer in CD_3COCD_3 (2.04 ppm), CD_2Cl_2 (5.32 ppm), or CD_3CN (1.93 ppm). IR spectra were recorded as KBr pellets with a Perkin-Elmer 1600 Series FTIR. UV–visible spectra were recorded in quartz cuvettes on a Cary 1E spectrophotometer. Electrochemical experiments were performed by using a BAS CV-27 cyclic voltammograph and a BAS Model RXY recorder. A three-compartment, gas-adapted cell was used with a platinum bead working electrode, a platinum wire auxiliary electrode, and a silver/silver chloride reference electrode. Cyclic voltammographs were recorded under N_2 in dry, distilled CH_2Cl_2 which was 0.1 M in supporting electrolyte (tetrabutylammonium hexafluorophosphate [TBAP]) and 2 mM in sample. The potentials are reported versus SCE. Elemental analysis for carbon, hydrogen, and nitrogen were carried out by Oneida Research Services, Whitesboro, NY.

All synthetic manipulations were carried out utilizing standard Schlenk techniques, and solvents were distilled from their appropriate drying agents.[24] Triethylamine (Aldrich) was distilled from CaH_2 and stored under an inert atmosphere. Ethanol (Sure-Seal; Aldrich), diethylamine (Aldrich), dimethyl sulfoxide (Fisher), catechol (Aldrich), 4-methylcatechol (Aldrich), phenylhydrazine hydrochloride (Aldrich), (4-bromophenyl)hydrazine hydrochloride (Aldrich), 1,1-diphenylhydrazine hydrochloride (Aldrich), $(CH_3CH_2)_4NCl$ (Aldrich), and other reagents were used as received without further purification. Silica gel (Merck grade 10181, 35–70 mesh) was purchased from Aldrich and utilized as chromatographic support. $ReOCl_3(PPh_3)_2$[25] and tetrabutylammonium hexafluorophosphate (TBAP) were synthesized by published procedures.[26] Selected analytical data for compounds **1** and **2** are presented in Table 1, while Table 2 summarizes data for compounds **5**–**7**.

Syntheses: **$[(CH_3CH_2)_4N]^+[ReO_2(O_2C_6H_4)_2]^-$ (1).** This complex was prepared by a modification of a procedure previously reported by Dilworth.[18] A solution of $ReOCl_3(PPh_3)_2$ (8.000 g; 9.60 mmol), catechol (2.714 g; 24.65 mmol) and diethylamine (5.930 g; 81.08 mmol) in 250 mL of absolute ethanol was heated to reflux. Upon heating, the yellow/green suspension became a dark green homogeneous reaction mixture. After 6 h reflux, the reaction mixture was transferred to an Erlenmeyer flask and cooled. Tetraethylammonium chloride (7.998 g; 48.27 mmol), dissolved in 10 mL of absolute ethanol, was added to the reaction mixture along with dimethyl sulfoxide (5.960 g; 76.30 mmol). The reaction mixture instantly turned purple and was allowed to stand for 12 h. The product was collected as deep purple needles by vaccum filtration and washed with ether and dried in air (4.553 g; 8.06 mmol; 81%). IR (KBr): 2985 (w), 1576 (m), 1466 (s), 1390 (w), 1281 (s), 1257 (vs), 1209 (w), 1173 (w), 1099 (w), 1014 (w), 1000 (w), 920 (vs), 887 (vs), 811 (s), 746 (vs), 654 (s), 605 (m), 531 (m). ^{1}H NMR (CD_3COCD_3, 293 K): δ 6.70 (m, 2H), 6.53 (m, 3H), 6.39 (m, 3H), 3.47 (q, 8H), 1.37 (t, 12H). ^{13}C NMR (CD_3COCD_3, 293 K): 149.4, 123.3, 117.9, 115.6, 114.8, 53.0, 7.6. UV–vis (λ_{max}, nm (ϵ, M^{-1} cm^{-1}) in CH_2Cl_2): 230 (2.3×10^4), 272 (1.8×10^4), 360 (5800), 450 (6600), 545 (7000).

$[(CH_3CH_2)_4N]^+[ReO_2(4\text{-}CH_3O_2C_6H_3)_2]^-$ (2). $ReOCl_3(PPh_3)_2$ (2.500 g; 3.00 mmol); 4-methylcatechol (0.956 g; 7.70 mmol), and diethylamine (1.854 g; 25.35 mmol) were mixed in 80 mL of absolute ethanol as described for **1**. Tetraethylammonium chloride (2.500 g; 15.09 mmol) dissolved in 30 mL of absolute ethanol and dimethyl sulfoxide (0.234 g; 3.00 mmol) were added to the cooled reaction mixture, and after 12 h of standing, a deep purple microcrystalline solid precipitated which was isolated as described for **1** (1.440 g; 2.43 mmol; 81%). Anal. Calcd for $C_{22}H_{32}NO_6Re$ (mol wt 592.71): C, 44.58; H, 5.44; N, 2.36. Found: C, 44.04; H, 5.44; N, 2.12. IR (KBr): 2982 (w), 1570 (m), 1477 (s), 1438 (m), 1398 (m), 1270 (vs), 1173 (w), 1121 (w), 1000 (w), 974 (w), 914 (vs), 883 (vs), 827 (s), 644 (s), 534 (s). ^{1}H NMR (CD_3COCD_3, 293 K): 6.58 (s, 1H), 6.56 (s, 1H), 6.32 (s, 1H), 6.30 (s, 1H), 6.24 (s, 1H), 6.22 (s, 1H), 3.46 (q, J = 7.3 Hz, 8H), 2.25 (s, 3H), 2.22 (s, 3H), 1.39 (t, 12H). ^{13}C NMR (CD_3CN, 293 K): 158.6, 156.5, 154.7, 149.4, 134.0, 128.3, 124.4, 119.1, 117.9, 116.4, 115.4, 115.2, 113.9, 52.9, 20.8, 20.4, 7.5. UV–vis (λ_{max}, nm (ϵ, M^{-1} cm^{-1}) in CH_2Cl_2): 210 (>2×10^4), 280 (1.8×10^4), 550 (4100).

$[(CH_3CH_2)_4N]^+[Re(NNC_6H_5)_2(O_2C_6H_4)_2]^-$ (5). To a suspension of **1** in 12 mL of anhydrous ethanol was charged a mixture of phenylhydrazine hydrochloride (0.646 g; 4.47 mmol) and triethylamine (0.489 g; 4.83 mmol) in 5 mL of anhydrous ethanol. The purple suspension turned wine-red upon addition of the hydrazine, and the reaction mixture

(15) Abrams, M. J.; Larsen, S. K.; Zubieta, J. *Inorg. Chim. Acta* **1990**, *171*, 133.
(16) Abrams, M. J.; Chen, Q.; Shaikh, S. N.; Zubieta, J. *Inorg. Chim. Acta* **1990**, *176*, 11.
(17) Abrams, M. J.; Larsen, S. K.; Zubieta, J. *Inorg. Chem.* **1991**, *30*, 2031.
(18) Abrams, M. J.; Larsen, S. K.; Shaikh, S. N.; Zubieta, J. *Inorg. Chem.* **1991**, *185*, 7.
(19) Schwartz, D. A.; Abrams, M. J.; Hauser, M. M.; Gaul, F. E.; Larsen, S. K.; Rauh, D.; Zubieta, J. *Bioconj. Chem.* **1991**, *2*, 333.
(20) Abrams, M. J.; Juweid, M.; ten Kate, C. I.; Schwartz, D. A.; Hauser, M. M.; Gaul, F. E.; Fuccello, A. J.; Rubin, R. H.; Strauss, H. W.; Fischman, A. J. *J. Nucl. Med.* **1990**, *31*, 2022.
(21) Kettler, P. B.; Abrams, M. J.; Chang, Y.-D.; Zubietta, J. *Inorg. Chim. Acta* **1994**, *218*, 157.
(22) Edwards, C. F.; Griffith, W. P.; White, A. J. P.; Williams, D. J. *J. Chem. Soc., Dalton Trans.* **1992**, 957.
(23) Dilworth, J. R.; Ibrahim, S. K.; Khan, S. R.; Hursthouse, M. B.; Karaulov, A. A. *Polyhedron* **1990**, *9*, 1323.
(24) Perrin, D. D.; Armarego, W. L. F.; Perrin, D. R. *Purification of Laboratory Chemicals*; Pergamon Press: New York, 1980.
(25) Parshall, G. W. *Inorg. Synth.* **1977**, *17*, 100.
(26) Osa, T.; Kuwana, T. *J. Electroanal. Chem.* **1969**, *22*, 389.

Table 1. Spectroscopic and Analytical Data for **1** and **2**

	analysis[a]			IR (cm^{-1})			UV−vis		
compd	C	H	N	ν_{CC}	ν_{CO}	ν_{ReO}	λ_{max} (nm)	ϵ (M^{-1} cm^{-1})	$E_{1/2}$[c]
1	40.3[b] (39.5)	5.3 (5.6)	2.5 (2.3)	1466	1257	920, 887	230, 272, 360, 450, 545	2.3×10^4, 1.8×10^4, 5800, 6800, 7000	−0.79[b]
2	44.04 (44.58)	5.44 (5.44)	2.12 (2.12)	1477	1270	914, 883	210, 280, 550	2.0×10^4, 1.8×10^4, 4100	−0.83

[a] Calculated values in parentheses. [b] Reference*. [c] At a platinum-bead working electrode using solutions 2×10^{-3} M in complex in 0.1 M $(Bu_4N)PF_6$ in CH_2Cl_2. All potentials are referred to SCE. Cyclic voltammograms were obtained at a sweep rate of 50 mV s^{-1}. $E_{1/2}$ estimated from $E_p^f - E_p^4/2$, which lies in the range 60−80 mV.

Table 2. Spectroscopic and Analytical Properties for **5**−**7**

	analysis[a]			IR (cm^{-1})			UV−vis		
compd	C	H	N	ν_{NN}	ν_{CC}	ν_{CO}	λ_{max} (nm)	ϵ (M^{-1} cm^{-1})	$E_{1/2}$ (V)[b]
5	50.56 (49.92)	5.13 (5.36)	9.00 (9.10)	1670, 1626, 1553	1470	1248	230, 267, 276, 360, 440, 530	2.8×10^4, 3.5×10^4, 3.9×10^4, 1.2×10^4, 7600, 5000	0.35, 0.67, 0.81
6	42.20 (42.67)	4.03 (3.98)	7.54 (7.78)	1662, 1601, 1541	1474	1252	230, 290, 360, 450, 565	3.1×10^4, 4.4×10^4, 1.5×10^4, 8600, 5400	0.19, 0.31, 0.70, 0.85
7	57.70 (57.67)	5.27 (5.31)	7.66 (7.59)	1586	1478	1249	230, 300, 317, 450	4.4×10^4, 4.6×10^4, 3.3×10^4, sh[c]	irrev[d]

[a] Calculated values in parentheses. [b] At a platinum-bead working electrode using solutions 2×10^{-3} M in complex in 0.1 M $(Bu_4N)PF_6$ in CH_2Cl_2. All potentials are referred to SCE. Cyclic voltammograms were obtained at a sweep rate of 50 mV s^{-1}. $E_{1/2}$ estimated from $E_p^f - E_p^r/2$, which lies in the range 60−80 mV. [c] Shoulder. [d] Irreversible oxidations.

was refluxed for 45 min. The reaction was then cooled to −20 °C overnight, and the crude product was collected by vacuum filtration on a filterstick and dried *in vacuo*. Recrystallization of the crude product from CH_2Cl_2/diethyl ether afforded large wine-red blocks (0.565 g; 0.76 mmol; 43%). Anal. Calcd for $C_{32}H_{38}N_5O_4Re$ (mol wt 742.89): C, 49.92; H, 5.36; N, 9.10. Found: C, 50.56; H, 5.13; N, 9.00. IR (KBr): 1676 (m), 1625 (m), 1582 (w), 1552 (s), 1474 (vs), 1333 (w), 1269 (sh), 1249 (vs), 1098 (w), 1016 (w), 907 (w), 866 (w), 797 (m), 763 (w), 743 (m), 682 (w), 641 (m), 628 (m), 562 (w), 526 (m). ^1H NMR (CD_3CN, 293 K): δ 7.49 (m, 8H), 7.25 (m, 2H), 6.74 (m, 2H), 6.47 (m, 4H), 6.35 (m, 2H), 3.13 (q, J = 7.3 Hz, 8H), 1.18 (t, 12H). ^{13}C NMR (CD_2Cl_2, 293 K): δ 160.0, 158.4, 148.0, 145.4, 129.8, 124.0, 119.1, 116.4, 114.8, 114.4, 46.1, 7.7. UV−vis (λ_{max}, nm (ϵ, M^{-1} cm^{-1}) in CH_2Cl_2): 230 (>2.8×10^4), 267 (>3.5×10^4), 276 (>3.9×10^4), 360 (1.2×10^4), 440 (7600), 530 (5000).

$[(CH_3CH_2)_4N]^+[Re(NNC_6H_4\text{-}4\text{-}Br)_2(O_2C_6H_4)_2]^-$ (6). A suspension of **1** (1.000 g; 1.77 mmol) in 12 mO of anhydrous ethanol was mixed with (*p*-bromophenyl)hydrazine hydrochloride (0.990 g; 4.43 mmol) and triethylamine (0.538 g; 5.32 mmol) in 20 mL of anhydrous ethanol as described for **5**. Recrystallization of the crude residue twice from CH_2Cl_2/ether afforded large wine-red columns (0.309 g; 0.35 mmol; 20%). Anal. Calcd for $C_{32}H_{36}Br_2N_5O_4Re$ (mol wt 900.68): C, 43.67; H, 4.03; N, 7.78. Found: C, 42.20; H, 3.98; N, 7.54. IR (KBr): 1662 (m), 1601 (s), 1570 (w), 1541 (s), 1474 (vs), 1269 (sh), 1252 (s), 1182 (w), 1143 (w), 1100 (w), 1067 (w), 1007 (w), 905 (w), 869 (w), 825 (sh), 799 (m), 732 (m), 646 (m), 524 (m). ^1H NMR (CD_2Cl_2, 293 K): δ 7.69 (b, 8H), 6.71 (m, 2H), 6.39 (m, 2H), 6.32 (m, 2H), 3.45 (q, J = 7.3 Hz, 8H), 1.36 (t, 12H). ^{13}C NMR (CD_2Cl_2, 293 K): δ 160.3, 145.3, 133.7, 126.2, 123.7, 199.9, 118.7, 117.0, 115.3, 114.9, 53.0, 7.7. UV−vis (λ_{max}, nm (ϵ, M^{-1} cm^{-1}) in CH_2Cl_2): 230 (>3.1×10^4), 290 (4.4×10^4), 360 (1.5×10^4), 450 (8800), 565 (5400).

$[(CH_3CH_2)_4N]^+[Re(NN(C_6H_5)_2)_2(O_2C_6H_4)_2]^-$ (7). To a suspension of **1** (0.400 g; 0.71 mmol) in 7 mL of anhydrous ethanol was charged 1,1-diphenylhydrazine hydrochloride (0.345 g; 1.56 mmol) and triethylamine (0.209 g; 2.07 mmol) in 8 mL of anhydrous ethanol as described for **5**. The crude product was recrystallized twice from CH_2Cl_2/ether to afford red-orange prisms (0.089 g; 0.099 mmol; 14%). Anal. Calcd for $C_{44.3}H_{48.6}Cl_{0.6}N_5O_4Re$ (mol wt 922.59): C, 57.67; H, 5.31; N, 7.59. Found: C, 57.70; H, 5.27; N, 7.66. IR (KBr): 3015 (w), 1586 (m), 1478 (vs), 1420 (w), 1344 (w), 1308 (w), 1249 (vs), 1158 (w), 1096 (w), 1018 (w), 868 (w), 796 (m), 756 (w), 726 (m), 692 (m), 638 (sh), 627 (m), 519 (m), 500 (w). ^1H NMR (CD_3CN, 293 K): δ 7.25 (m, 16H), 7.09 (m, 4H), 6.46 (m, 2H), 6.29 (m, 4H), 6.04 (m, 2H), 3.13 (q, J = 7.3 Hz), 1.18 (t, 12H). ^{13}C NMR (CD_2Cl_2, 293 K): 131.2, 128.9, 125.1, 122.1, 121.8, 120.7, 104.9, 61.07.7. UV−vis (λ_{max}, nm (ϵ, M^{-1} cm^{-1}) in CH_2Cl_2): 230 (>4.4×10^4), 300 (4.6×10^4), 317 (3.3×10^4), 450 (sh).

$Na[Re(NN(C_6H_5))_2(O_2C_6H_4)_2]\cdot CH_3CN$ (8). A known quantity of **5** (0.150 g; 0.20 mmol) was eluted down a column of silica gel using a 3:1 mixture of toluene/methanol as the eluant. Rotary evaporation of the colored fractions afforded a red microcrystalline solid (0.024 g; 0.0038 mmol; 19%). Anal. Calcd for $C_{24}H_{20}N_4NaO_5Re$ (mol wt 635.63): C, 44.10; H, 3.08; N, 8.57. Found: C, 44.56; H, 3.02; N, 8.50. IR (KBr): 1701 (m), 1642 (vs), 1584 (sh), 1561 (s), 1479 (vs), 1273 (sh), 1250 (s), 1100 (w), 1020 (w), 798 (m), 757 (w), 736 (m), 682 (m), 648 (m), 614 (sh), 574 (w), 532 (w). ^1H NMR (CD_3CN, 293 K): δ 7.49 (m, 8H), 7.25 (m, 2H), 6.74 (m, 2H), 6.47 (m, 4H), 6.35 (m, 2H). UV−vis (λ_{max}, nm (ϵ, M^{-1} cm^{-1}) in CH_2Cl_2 and H_2O): 260 (6400), 290 (7500), 350 (sh), 430 (sh), 510 (sh).

Table 3. Crystallographic Data for the Structural Studies of $(Et_4N)[Re(NNPh)_2(O_2C_6H_4)_2]$ (**5**), $(Et_4N)[Re(NNPh_2)_2(O_2C_6H_4)_2]$ (**7**), and $Na[Re(NNPh)_2(O_2C_6H_4)_2]\cdot CH_3CN$ (**8**)

	5	**7**	**8**
chemical formula	$C_{32}H_{38}N_5O_4Re$	$C_{44}H_{48}N_5O_4Re$	$C_{26}H_{18}N_5NaO_4Re$
a, Å	14.458(3)	11.660(2)	5.785(1)
b, Å	10.436(2)	11.864(2)	9.670(2)
c, Å	21.767(4)	15.400(2)	23.142(5)
α, °		107.12(3)	
β, °	107.04(3)	94.99(3)	90.91(3)
γ, °		97.61(3)	
V, Å^3	3140(2)	2000(1)	1294.4(7)
Z	4	2	2
formula weight	742.9	897.1	676.7
space group	$P2_1/c$	$P\bar{1}$	$P2/n$
T, °C	−60	−60	−60
λ, Å	0.71073	0.71073	0.71073
D_{calc}, g cm^{-3}	1.572	1.490	1.737
D_{obs}, g cm^{-3}	1.56(1)	1.47(1)	1.74(1)
μ, cm^{-1}	39.12	30.86	47.52
R^a	0.0532	0.0534	0.0494
R_w[b]	0.0686	0.0681	0.0616

[a] $\sum||F_o| - |F_c||/\sum|F_o|$. [b] $[\sum w(|F_o| - |F_c|)^2/\sum w|F_o|^2]^{1/2}$.

X-ray Crystallography. The compounds **5**, **7**, and **8** were studied using a Rigaku AFC5S diffractometer, equipped with a low-temperature device. Since the crystals degraded slowly at room temperature, data collection was carried out at 213 K. Crystal stability was monitored using five medium intensity reflections in each case, and no significant changes in the intensities of the standards were observed over the course of the data collections. The crystal parameters and other experimental details of the data collections are summarized in Table 3. A complete description of the crystallographic methods is given in the supplementary materials. Atomic positional parameters are listed in Tables 4, 5, and 6 for **5**, **7**, and **8**, respectively.

The structures were solved by the Patterson method and refined by full-matrix least squares. The details of the structure solutions and

Table 4. Atomic Positional Parameters ($\times 10^4$) for $(Et_4N)[Re(NNPh)_2(O_2C_6H_4)_2]$ (**5**)

	x	y	z
Re(1)	7671(1)	2271(1)	−76(1)
O(1)	6903(5)	1372(7)	445(4)
O(2)	7760(6)	3573(7)	621(4)
O(3)	6439(5)	3189(7)	−568(4)
O(4)	7111(6)	989(7)	−757(4)
N(1)	8389(7)	3288(10)	−444(5)
N(2)	8924(7)	4104(10)	−541(5)
N(3)	8711(7)	1278(9)	292(5)
N(4)	9354(7)	495(10)	458(5)
N(5)	7023(9)	7303(21)	−32(7)
C(1)	6787(8)	2020(11)	930(5)
C(2)	7230(8)	3263(11)	1024(5)
C(3)	7132(9)	4056(12)	1503(6)
C(4)	6563(9)	3671(12)	1890(6)
C(5)	6143(10)	2485(11)	1797(6)
C(6)	6249(8)	1669(12)	1322(5)
C(7)	5900(9)	2533(11)	−1083(6)
C(8)	6235(9)	1347(11)	−1190(6)
C(9)	5727(9)	573(12)	−1692(6)
C(10)	4870(10)	992(13)	−2092(7)
C(11)	4542(12)	2156(14)	−1997(8)
C(12)	5023(10)	2987(13)	−1550(6)
C(13)	9050(9)	4166(11)	−1169(6)
C(14)	8396(10)	3686(14)	−1709(7)
C(15)	8576(12)	3847(15)	−2308(8)
C(16)	9403(11)	4455(14)	−2333(8)
C(17)	10066(10)	4922(13)	−1796(7)
C(18)	9893(9)	4808(12)	−1203(6)
C(19)	10127(9)	697(12)	−1021(6)
C(20)	10800(10)	−234(14)	1212(7)
C(21)	11605(11)	−37(15)	1730(7)
C(22)	11724(10)	1086(13)	2050(7)
C(23)	11062(11)	2033(14)	1891(7)
C(24)	10230(10)	1836(13)	1365(7)
C(25)	1207(12)	2625(14)	99(8)
C(26)	3458(13)	3699(18)	1160(9)
C(27)	3566(22)	3926(28)	−52(14)
C(28)	3445(26)	2528(29)	793(17)
C(29)	4755(37)	3137(43)	46(24)
C(30)	2359(13)	1633(18)	−1088(9)
C(31)	3715(22)	1471(28)	83(14)
C(32)	2002(55)	2989(66)	−239(36)

refinements are presented in the supplementary materials. No anomalies were encountered in the refinements of the structures. Bond lengths and angles for the structures of **5**, **7**, and **8** are listed in Table 7.

Results and Discussion

Synthesis and Spectroscopic Characterization of *cis*-Dioxorhenium(VII) Catecholate Complexes. The hydrazido−catecholate precursor $[(CH_3CH_2)_4N]^+[ReO_2(cat)_2]^-$ (**1**) was prepared by a modification of a method previously described by Dilworth[23] (eq 1). The precursor, $ReOCl_3(PPh_3)_2$, was heated

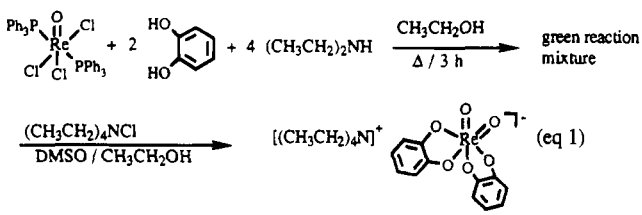

(eq 1)

to reflux in absolute ethanol in the presence of a stoichiometric amount of catechol and excess base (diethylamine) to generate a dark green reaction mixture (presumably, the rhenium(V) monooxo catecholate intermediate).[21] This reaction mixture was cooled, and DMSO was added to act as an oxo transfer agent. Upon addition of DMSO, the reaction mixture turned intense purple, and a large cation ($(CH_3CH_2)_4NCl$) was added to

Table 5. Atomic Positional Parameters ($\times 10^4$) for $(Et_4N)[Re(NNPh_2)_2(O_2C_6H_6)_3]$ (**7**)

	x	y	z
Re(1)	2305(1)	3532(1)	2103(1)
O(1)	3142(7)	2945(8)	3049(5)
O(2)	3675(7)	2976(8)	1455(5)
O(3)	3354(7)	5080(8)	2854(5)
O(4)	1259(7)	4235(8)	3054(5)
N(1)	1991(9)	4181(10)	1230(7)
N(2)	2165(9)	4780(9)	631(6)
N(3)	1235(9)	2226(10)	1730(7)
N(4)	378(8)	1399(9)	1756(7)
C(1)	4027(11)	2376(12)	2757(9)
C(2)	4309(11)	2365(11)	1890(8)
C(3)	5192(12)	1802(13)	1529(10)
C(4)	5792(13)	1234(14)	2028(10)
C(5)	5525(14)	1218(15)	2894(11)
C(6)	4643(12)	1796(13)	3262(10)
C(7)	2834(12)	5810(13)	3486(10)
C(8)	1701(12)	5331(13)	3592(9)
C(9)	1109(14)	5981(14)	4271(10)
C(10)	1643(15)	7173(16)	4804(12)
C(11)	2735(16)	7643(17)	4680(12)
C(12)	3335(15)	6981(15)	4026(11)
C(13)	3066(11)	5815(12)	866(8)
C(14)	3107(12)	6744(12)	1632(9)
C(15)	3969(13)	7753(14)	1820(11)
C(16)	4782(14)	7793(15)	1207(11)
C(17)	4714(13)	6838(14)	438(10)
C(18)	3871(11)	5865(12)	250(9)
C(19)	1466(10)	4329(11)	−247(8)
C(20)	1140(11)	5105(12)	−697(9)
C(21)	422(11)	4672(12)	−1516(9)
C(22)	19(13)	3482(14)	−1903(11)
C(23)	317(15)	2712(17)	−1451(12)
C(24)	1078(13)	3139(14)	−604(10)
C(25)	474(11)	804(11)	2456(8)
C(26)	−419(13)	705(13)	2947(10)
C(27)	9676(15)	79(14)	3616(11)
C(28)	736(16)	−363(16)	3711(12)
C(29)	1621(14)	−222(14)	3254(10)
C(30)	1495(12)	389(12)	2607(9)
C(31)	−627(10)	1067(11)	1071(8)
C(32)	−859(13)	1836(14)	619(10)
C(33)	−1845(16)	1525(15)	−60(12)
C(34)	2570(12)	9585(13)	292(10)
C(35)	7695(12)	9569(13)	157(9)
C(36)	−1275(12)	−46(13)	843(9)
N(5)	2855(34)	3436(35)	−4443(26)
C(37)	2299(44)	3922(47)	−4765(33)
C(38)	1721(18)	2927(19)	−5173(14)
C(39)	2439(30)	2727(31)	−3401(23)
C(40)	3285(51)	1702(53)	−3711(41)
C(41)	3979(24)	4639(25)	−3061(20)
C(42)	3957(19)	4606(20)	−2114(16)
C(43)	1879(24)	4662(25)	−3303(19)
C(44)	1951(22)	6095(22)	−3149(16)

precipitate the product as crystalline purple needles in high yield. Selected analytical and spectroscopic data is presented in Table 1. The infrared spectrum for **1** exhibits intense ν_{CC} and ν_{CO} stretches for the coordinated catecholate ligands at 1467 and 1257 cm^{-1}, respectively. The ν_{CC} stretch corresponds to the ring stretch between C(1) and C(2) of the catecholate ring and shifts markedly to lower energy from 1620 cm^{-1} for catechol[26] upon deprotonation of the catecholate oxygen donor atoms and the subsequent coordination of the catecholate ligand.[23] The absence of any ν_{OH} bands confirms that the oxygen donor atoms in the catecholate ligands are fully deprotonated. In addition, two ν_{ReO} stretches are observed at 920 cm^{-1} (ν_s) and at 887 cm^{-1} (ν_{as}) which is typical of complexes that contain two oxo groups in a *cis* configuration.[27-30,39] These values are in contrast

(27) Grearies, S. J.; Griffith, W. P. *Spectrochim. Acta* **1991**, *47A*, 133.

Table 6. Atomic Positional Parameters ($\times 10^4$) for $Na[Re(NNPh)_2(O_2C_6H_4)_2]\cdot CH_3CN$ (**8**)

	x	*y*	*z*
Re(1)	2500	8902(1)	7500
O(1)	9094(16)	2669(8)	2960(3)
O(2)	5055(15)	1497(8)	3082(3)
N(1)	9263(20)	−159(10)	2890(4)
N(2)	10733(18)	−887(10)	3110(4)
C(1)	7751(20)	3168(12)	3388(5)
C(2)	5679(21)	2533(12)	3458(5)
C(3)	4148(22)	2939(12)	3887(5)
C(4)	4812(23)	4078(14)	4236(6)
C(5)	6866(23)	4697(15)	4164(6)
C(6)	8438(22)	4285(12)	3740(5)
C(7)	10473(19)	−1285(10)	3705(4)
C(8)	12167(23)	−2060(13)	3940(5)
C(9)	12064(27)	−2447(16)	4515(6)
C(10)	10224(24)	−2079(14)	4832(6)
C(11)	8492(23)	−1302(13)	4605(5)
C(12)	8579(21)	−897(12)	4027(5)
Na(1)	12500	2987(7)	2500
N(3)	12500	5465(20)	2500
C(13)	5000	3944(33)	7500
C(14)	2500	3537(37)	7500

Table 7. Selected Bond Lengths (Å) and Angles (deg) for the Structures of $(Et_4N)[Re(NNPh)_2(O_2C_6H_4)_2]$ (**5**), $(Et_4N)[Re(NNPh_2)_2(O_2C_6H_4)_2]$ (**7**), and $Na[Re(NNPh)_2(O_2C_6H_4)_2]\cdot CH_3CN$ (**8**)

	5	**7**	**8**
Re1−O1	2.034(9)	2.023(10)	2.064(8)
Re1−O2	2.013(8)	2.037(8)	2.006(8)
Re1−O3	2.030(7)	2.029(7)	
Re1−O4	1.984(7)	2.046(8)	
Re1−N1	1.825(11)	1.770(12)	1.817(10)
Re1−N3	1.809(9)	1.768(10)	
O1−C1	1.31(2)	1.35(2)	1.36(1)
O2−C6	1.30(1)	1.36(2)	1.37(1)
O3−C7	1.36(1)	1.35(2)	
O4−C12	1.39(1)	1.33(2)	
N1−N2	1.21(2)	1.33(2)	1.21(1)
N3−N4	1.21(1)	1.32(2)	
Na1−O1			2.276(9)
Na1−O2			2.451(9)
Na1−N3			2.39(2)
O1−Re1−O2	79.4(3)	79.4(3)	80.0(3)
O3−Re1−O4	79.7(3)	79.1(3)	
O1−Re1−O3	88.5(3)	80.5(4)	85.2(4)
O1−Re−O4	86.3(3)	88.4(4)	
O1−Re−N1	170.5(4)	163.4(4)	172.3(4)
O1−Re−N3	90.4(4)	92.2(5)	93.8(4)
O2−Re−O3	86.0(3)	89.7(3)	83.7(3)
O2−Re−O4	160.0(3)	164.7(3)	157.8(4)
O2−Re−N1	91.1(4)	87.3(4)	89.6(4)
O2−Re−N3	101.1(4)	102.4(4)	
O3−Re−N1	91.0(4)	89.7(4)	
O3−Re−N3	172.5(4)	163.4(4)	
O4−Re−N1	103.0(4)	102.9(4)	101.1(4)
O4−Re−N3	92.8(4)	87.2(4)	
N1−Re−N3	91.3(5)	100.3(5)	96.0(6)
Re−N1−N2	163.9(9)	159.6(8)	169.5(10)
Re−N3−N4	170.0(9)	159.7(8)	
N1−N2−C13	117.8(10)	119.9(9)	118.4(10)
N1−N2−C19		117.9(9)	
N3−N4−C25(19)	120.0(11)	119.9(9)	
N3−N4−C31		119.3(11)	

to the values previously reported by Dilworth.[23] ^1H and ^{13}C NMR spectra also support the assertion that **1** maintains its *cis*-dioxo geometry in solution by showing four overlapping resonances in the catecholate region (δ 6.2−7.0) and six inequivalent ^{13}C catecholate resonances in the aromatic region. The chemical shifts of C(1) and C(2) of the catecholate rings are in the region expected for catecholate ligands (δ 155−165), while coordinated quinone ligands exhibit resonances in the range δ 180−200.[22] The electronic absorption spectrum of **1** displays two intense bands in the UV region at 230 and 272 nm indicative of $\pi\rightarrow\pi^*$ transitions in the catechol ligands and three bands in the visible region at 360, 450, and 545 nm, indicative of ligand to metal charge transfer bands.

The analogous *cis*-dioxo bis(catecholate) species with 4-methylcatechol (**2**) was prepared in a similar fashion in high yield. Selected spectroscopic and analytical data for this complex is presented in Table 1. ^1H and ^{13}C NMR data reveal two distinct singlets in the tolyl region in the ^1H NMR spectrum (δ 2.25 and 2.22) in approximately a 3:2 ratio, suggesting two possible isomers occurring in solution (**2A** and **2B**).

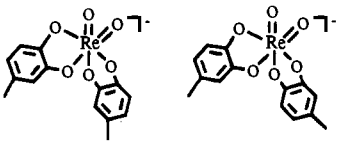

2A **2B**

The IR spectrum of **2** shows two stretches for the catecholate ligands at 1477 (ν_{CC}) and 1270 cm^{-1} (ν_{CO}) and two νReO stretches at 914 (ν_s) and 883 cm^{-1} (ν_{as}), indicative of a *cis*-dioxo geometry. The UV−visible spectrum is quite similar to **1**, revealing intense $\pi\rightarrow\pi^*$ transitions in the UV region for the catecholate ligands and a ligand to metal charge transfer band in the visible region (550 nm; ϵ 4100).

Cyclic voltammetry for complex **2** reveals a reversible reduction at −0.83 V (vs SCE). This reduction is assigned to the rhenium metal center since the catecholate ligands are already in their fully reduced state. Also, this value is in agreement with reduction potentials measured for **1** (−0.79 V), $[(CH_3CH_2)_4N]^+[ReO_2(O_2C36H_3Bu^t)_2]^-$ (**3**) (−0.88 V), and $[(CH_3CH_2)_4N]^+[ReO_2(O_2C_6H_2Bu^t_2)_2]1-$ (**4**) (−1.01 V) where these complexes become increasingly more difficult to reduce with increasing alkyl substitution. Controlled potential electrolysis of **2** in CH_2Cl_2 resulted in passage of 1 F/mol of **2**, and the EPR spectrum of this solution revealed a broad featureless signal with no observable hyperfine coupling at either 298 or 183 K. Similar EPR spectra were observed in other rhenium(VI) complexes which show only broad signals at 298 K.[31-34] However, this in stark contrast to the EPR spectrum of the tris(catecholato)rhenium(VI) complexes reported by Pierpont where a six-line pattern is observed at 298 K with hyperfine coupling to the $I = 5/2$ isotopes ^{185}Re and ^{187}Re.[35,36]

Synthesis and Spectroscopic Characterization of Rhenium Hydrazino−Catecholate Complexes. Dilworth[23] previously reported that the attempted syntheses of rhenium hydrazino−catecholate complexes by the reaction of monosubstituted or 1,1-disubstituted organohydrazines with **1** led to discernible color changes, but isolation of any products was not achieved.

(28) Herrmann, W. A.; Küsthardt, U.; Hudtwich, E. *J. Organomet. Chem.* **1985**, *294*, 633.
(29) Takacs, J.; Kiprof, P.; Riede, J.; Herrmann, W. A. *Organometallics* **1990**, *9*, 782.
(30) Takacs, J.; Cooks, M. R.; Kiprof, P.; Kuchler, J. G.; Herrmann, W. A. *Organometallics* **1991**, *10*, 376.
(31) Baldas, J.; Boas, J. F.; Bonnyman, J.; Pilbrew, J. R.; Williams, G. A. *J. Am. Chem. Soc.* **1985**, *107*, 1886.
(32) Al-Mowali, A. H.; Porte, A. L. *J. Chem. Soc., Dalton Trans.* **1975**, 250.
(33) Gibson, J. F.; Lack, G. M.; Mertis, K.; Wilkinson, G. *J. Chem. Soc., Dalton Trans.* **1976**, 1492.
(34) Holloway, J. H.; Raynes, J. B. *J. Chem. Soc., Dalton Trans.* **1975**, 737.
(35) de Learie, L. A.; Haltiwanger, R. C.; Pierpoint, C. G. *Inorg. Chem.* **1987**, *26*, 817.
(36) deLearie, L. A.; Pierpoint, C. G. *J. Am. Chem. Soc.* **1986**, *108*, 6393.

However, under our conditions, when **1** was reacted with an excess of an organohydrazine in refluxing ethanol, rhenium hydrazino−catecholate complexes were isolated (eq 2). These

$$[(CH_3CH_2)_4N][ReO_2(O_2C_6H_4)_2] + 2.5R^1R^2NNH_2{\cdot}HCl + 2.5(CH_3CH_2)_3N \xrightarrow[\Delta/1\ h]{CH_3CH_2OH} [(CH_3CH_2)_4N][Re(N_2R^2)_2(O_2C_6H_4)_2]\ (\mathbf{5}, \mathbf{6}) + [(CH_3CH_2)_4N][Re(N_2R^1R^2)_2(O_2C_6H_4)_2]\ (\mathbf{7}) \quad (2)$$

$R^1 = H, R^2 = C_6H_5$ (**5**); $R^1 = H, R^2 = 4\text{-}BrC_6H_4$ (**6**); $R^1 = R^2 = C_6H_5$ (**7**)

complexes were isolated by recrystallization of the crude product from CH_2Cl_2/ether as either maroon-red (**5**, **6**) or orange-red (**7**) crystalline solids. Selected analytical and spectroscopic data for these complexes is presented in Table 2. Attempted syntheses of oxo−diazenido or oxo−hydrazido complexes by addition of 1 equiv of the appropriate organohydrazine led to the formation of 0.5 equiv of this bis(diazenido) or bis(hydrazido) complexes, respectively. Also, attempts to protonate **5** with either HBF_4 or HCl/ether led to intractable products. This phenomenon was also observed rhenium diazenido−thiolate complexes where the thiolate ligand was more susceptible to protonation than either the N_α or N_β atoms of the diazenido ligand.[37] This may also be the case for **5**, where the catecholate ligands are also more susceptible to protonation. Additionally, the reaction of **1** with chelating organohydrazines such as benzoylhydrazine led to intractable products.

The infrared spectra of **5** and **6** display three intense ν_{NN} bands between 1550 and 1670 cm^{-1} which are indicative of the symmetric and asymmetric stretches commonly observed in a *cis*-bis(diazenido) moiety.[38] Intense catecholate bands are also observed in these complexes at 1470−1474 cm^{-1} (ν_{CC}) and 1248−1252 cm^{-1} (ν_{CO}). For the bis(hydrazido) complex **7**, a single ν_{NN} stretch is observed at 1586 cm^{-1}. No ν_{ReO} bands were observed for **5**, **6**, or **7**, confirming displacement of the oxo groups by the hydrazino ligands.

^1H NMR spectroscopy gave sharp and nonisotropically shifted resonances indicating that these complexes (**5**−**7**) are diamagnetic. The aromatic resonances appear at their usual positions for the hydrazino and catecholate ligands, and resonances are observed for the tetraethylammonium cation which are consistent with the proposed formulations of **5**−**7**. ^{13}C NMR spectroscopy for **5**−**7** show the correct number of resonances, consistent with the *cis* geometry of the hydrazino ligands. The chemical shift of the O-bound carbons of the catecholate ligands (C(1,2)) are in the chemical shift region (δ 158−160) expected for coordinated catecholate ligands in contrast to those for coordinated quinone ligands (δ 180−200). The resonances for C(1,2) are not observed in **7**, but the catecholate nature of the ligands is unambiguously confirmed by an X-ray crystal structure (*vide infra*). The expected resonances are also observed for the tetraethylammonium cation in each of these complexes.

The UV−visible spectra for **5**−**7** show two or three intense bands in the UV region indicative of $\pi \rightarrow \pi^*$ transitions of the catecholate ligands and/or in the phenyl rings of the hydrazino ligands. In the diazenido complexes (**5** **6**), three intense bands are observed in the visible region at 360, 440−450, and 560−565 nm which are assigned as ligand to metal charge transfer bands. Specific assignment is not possible since bands in these regions are also observed in **1** and **2**. However, with the hydrazido complex **7**, only a broad shoulder is observed in the visible region.

Cyclic voltammetry measurements of the diazenido complexes **5** and **6** exhibit four successive ligand-centered one-electron oxidations as shown in Table 2. These oxidation waves are assigned to the catecholate ligands from a controlled potential coulometry experiment performed on **5**. The one-electron oxidation of a solution of **5** by controlled potential coulometry followed by EPR spectroscopy displays a very sharp isotropic signal at $g_{iso} = 2.014$ with a line width of 10 G. In comparison to the analogous experiment performed with **2** (*vide supra*) where a one-electron reduction was metal-centered and displayed a broad, featureless EPR spectrum, this signal is probably indicative of a organic radical.

By way of contrast, the cyclic voltammogram for **7** shows two irreversible oxidations. This may reflect the different electronic properties of the diazenido ligand (**A**) of **5** and **6**, a formally 1+ ligand, and the hydrazido ligand (**B**) of **7**, a formally 2− ligand. In a formal sense, the oxidation state of

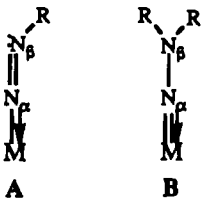

the rhenium metal centers in **5** and **6** could arguably be assigned as I while for **7** an oxidation state of VII would be expected. The diamagnetism of these complexes is in agreement with such assignments, but such a wide variance in oxidation state for these complexes, prepared by very similar methods and undergoing ligand substitution by similar reaction mechanism (i.e., condensation), is certainly disputable.

The Formation of $Na^+[Re(N_2(C_6H_5))_2(cat)_2]^-$ (8) from 5. In an attempt to purify **5**, a 3:1 solution of **5** in toluene/methanol was eluted down a column of silica gel (Merck grade 10181; 35−70 mesh size) as an intense red band. ^1H NMR spectroscopy of the red product exhibits resonances in the exact positions as they appear in **5**, with the exception that the resonances for the tetraethylammonium cation have disappeared. The IR spectrum for the red product is also nearly identical to **5**. Since there are no observable δ_{NH} resonances in the ^1H NMR spectrum or ν_{NH} stretches in the IR spectrum, protonation of the N_α or N_β atoms of the phenyldiazenido ligand was not considered. As expected, the UV−visible spectrum was not substantially different from that of **5** (see Table 2). Cation exchange of the tetraethylammonium cation by a sodium (Na^+) cation was confirmed unambiguously by X-ray crystallography (*vide infra*). Since the silica gel utilized as the support in the column contains between 150 and 300 ppm sodium (as $Na_2SiO_3{\cdot}5H_2O$) (39), cation exchange of this type is feasible. As a sodium salt, **8** has substantial water solubility. Since the UV−visible band shape of **8** in H_2O is identical to that in CH_2Cl_2, one can postulate that the Re=N=N(C_6H_5) chromophore is stable in water. This result has implications for protein labeling in that the M=N=NR linkage at one terminus of the bifunctional chelate−protein adduct exhibits some degree of stability under physiological conditions and lends credence to the bifunctional chelate linkage remaining intact during tracer (medical) applications.

Description of Structural Properties. The structure of $(Et_4N)[Re(NNPh)_2(O_2C_6H_4)_2]$ (**5**) consists of discrete Et_4N^+

(37) Nicholson, T.; Zubieta, J. *Inorg. Chim. Acta* **1985**, *100*, 235.
(38) Johnson, B. F. G.; Haymore, B. L.; Dilworth, J. R. In *Comprehensive Coordination Chemistry*; Wilkinson, G., Gillard, R. D., McCleverty, J. A., Eds.; Pergamon Press: Oxford, 1989; Chapter 133, p 99.

Table 8. Comparison of Selected Structural Features of Complexes with the $\{M(NNR)_2\}$ and $\{M(NNR_2)_2\}$ Cores

complex	M−N	N−N	M−N−N	N−M−N	ref
		a. Six-Coordinate Geometry			
$(Et_4N)[Re(NNPh)_2(O_2C_6H_4)_2]$ (**5**)	1.83(1)	1.21(2)	163.9(9)	91.3(5)	this work
	1.81(1)	1.20(1)	170.0(9)		
$Na[Re(NNPh)_2(O_2C_6H_4)_2]\cdot CH_3CN$ (**8**)	1.82(1)	1.21(1)	172.3(4)	96.0(6)	this work
$(Et_4N)[Re(NNPh_2)_2(O_2C_6H_4)_2]$ (**7**)	1.77(1)	1.33(2)	159.6(8)	100.3(5)	this work
	1.77(1)	1.32(2)	159.7(8)		
$[Re(NNMePh)_2(S_2CNMe_2)_2]BPh_4$	1.78(1)	1.30(1)	1.66.6(8)	104.5(4)	42
	1.78(1)	1.29(1)	1.66.9(9)		
$[Mo(NNPh_2)_2(S_2CNMe_2)_2]$	1.790(8)	1.31(1)	169.9(8)	107.5(3)	43
$[Mo(NNAr)_2(S_2N_2C_8H_{18})]$	1.81(1)	1.23(2)	170(2)	95.5	44
	1.82(2)	1.20(2)	168(2)		
$[Mo_2(NNPh)_4(acac)_2(OMe)_2]$	1.832(9)	1.216(14)	173.3(9)	94.7	45
		b. Trigonal-Bipyramidal Geometry			
$[TcCl(NNAr)_2(PPh_3)_2]$	1.796(6)	1.229(9)	170.7(7)	118.4(3)	46
	1.783(7)	1.224(8)	166.2(6)		
$[MoCl(NNMe_2)_2(PPh_3)_2]^+$	1.752(5)	1.291(7)	163.8(4)	112.2(2)	43

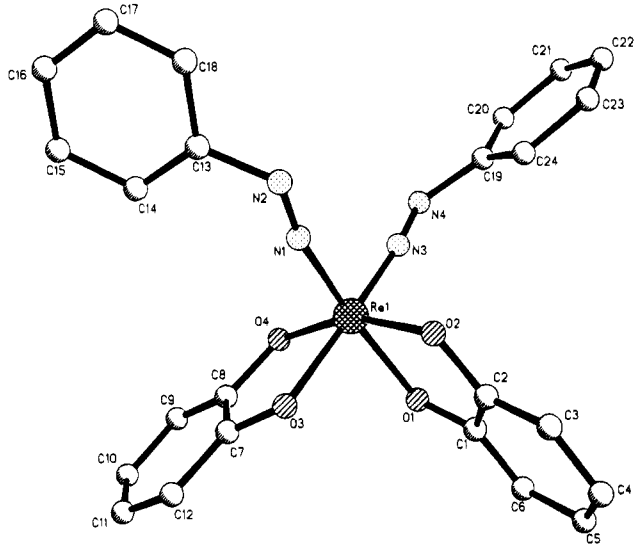

Figure 1. View of the structure of $[Re(NNPh)_2(O_2C_6H_4)_2]^{1-}$, showing the atom labeling scheme.

cations and $[Re(NNPh)_2(O_2C_6H_4)_2]^-$ molecular anions. As shown in Figure 1, the anion of **5** possesses distorted octahedral geometry with equivalent aryldiazenido groups adopting mutually *cis* orientation and the oxygen donors of the bidentate catecholate ligands occupying the remaining coordination sites. The aryldiazenido units display nearly linear geometry, with Re1−N_α−N_β angles of 163.9(9)° and 170.0(9)°. The short Re−N and N−N distances associated with *cis*-$[Re(NNPh)_2]$ unit reflect multiple bonding delocalized throughout the unit and are comparable to M−N and N−N bond distances previously reported for complexes with analogous $\{M(NNR)_2\}$ units (Table 8). The N−Re−N angle of 91.3(5)° is significantly compressed relative to the corresponding valence angles between π-bonding ligands in six coordinate species containing *cis*-$\{MO_2\}$ or *cis*-$\{MO(NNR)\}$ units (M = Mo, Re): 107−112° and 108−114° ranges, respectively.[38,40−42] This characteristic feature of the *cis*$\{M(NNR)_2\}$ unit reflects an interaction between the α-nitrogens[43] or may be related to the steric requirements of the two catecholato ligands.[44−46]

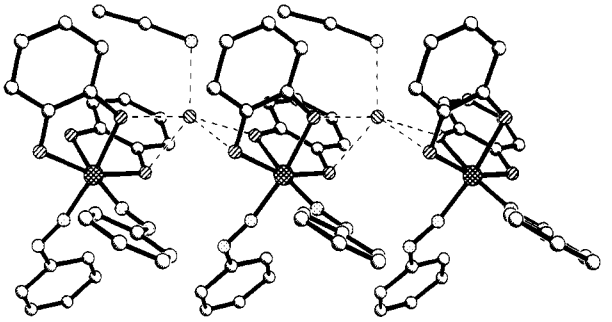

Figure 2. One-dimensional chains present in the structure of $Na(CH_3CN)[Re(NNPh)_2(O_2C_6H_4)_2]$ (**8**).

The structure of the anion of $Na[Re(NNPh)_2(O_2C_6H_4)_2]\cdot CH_3CN$ (**8**) is, not unexpectedly, essentially identical to that of **5**. The unusual feature of the structure of **8** (Figure 2) is the presence of Na^+ cations which serve to bridge adjacent pairs of $[Re(NNPh)_2(O_2C_6H_4)_2]^-$ anions so as to produce $\{Na[Re(NNPh)_2(O_2C_6H_4)_2]^-\}_\infty$ infinite chains running parallel to the crystallographic *c* axis. The Na^+ adopts a distorted five-coordinate geometry as a consequence of interactions with four oxygens from different catecholate ligands of each of two adjacent $[Re(NNPh)_2(O_2C_6H_4)_2]^-$ anions and with the nitrogen of the acetonitrile molecule of crystallization.

The structure of $(Et_4N)[Re(NNPh_2)_2(O_2C_6H_4)_2]$ (**7**) consists of discrete Et_4N^+ cations and $[Re(NNPh_2)_2(O_2C_6H_4)_2]^-$ anions. As shown in Figure 3, the molecular anion of **7** exhibits distorted octahedral geometry defined by the four oxygen donors of two *cis*-catecholato ligands and the nitrogen donors of the phenylhydrazido(2−) groups in the *cis* orientation. As shown in Table 8, the metrical parameters for the $\{Re(NNPh_2)_2\}$ unit are similar to those reported for other examples of octahedral complexes with the $\{M(NNR)_2)_2\}$ core and indicative of significant delocalized multiple bond character throughout the unit.[41]

Comparison of the bonding parameters associated with the $\{Re(NNPh)_2\}$ and $\{Re(NNPh_2)_2\}$ cores of **5**, **7**, and **8** with those for previously reported examples of complexes with the $\{M(NNR)_2\}$ and $\{M(NNR_2)_2\}$ cores and metals of comparable covalent radii to that of rhenium reveal distinct structural characteristics for the *cis*-bis(diazenido) and *cis*-bis(hydrazido) cores. References to the six-coordinate complexes listed in Table 8 illustrates that the M−N and N−N bond lengths for the *cis*-$\{M(NNR)_2\}$ cores fall in the ranges 1.81−1.84 and

(39) Schneider, R. Personal communication, Aldrich Chemical Co., Milwaukee, WI.
(40) Nugent, W. A.; Mayer, J. M. *Metal-Ligand Multiple Bonds*; Wiley-Interscience: New York, 1988.
(41) Enemark, J. H.; Feltham, R. D. *Coord. Chem. Rev.* **1974**, *13*, 339.
(42) Dilworth, J. R.; Jobanputra, P.; Parrott, S. J.; Thompson, R. M. *Polyhedron* **1992**, *11*, 147.
(43) Chatt, J.; Crichton, B. A. L.; Dilworth, J. R.; Dahlstrom, P.; Gutkoska, R.; Zubieta, J. *Inorg. Chem.* **1982**, *21*, 2383.
(44) Dahlstrom, P. L.; Dilworth, J. R.; Shulman, P.; Zubieta, J. *Inorg. Chem.* **1982**, *21*, 933.
(45) Caviello, D.; Gouzerh, P.; Jeannin, Y. *Nourv. J. Chim.* **1985**, *9*, 749.
(46) Nicholson, T.; deVries, N.; Davison, A.; Jones, A. G. *Inorg. Chem.* **1989**, *28*, 3183.

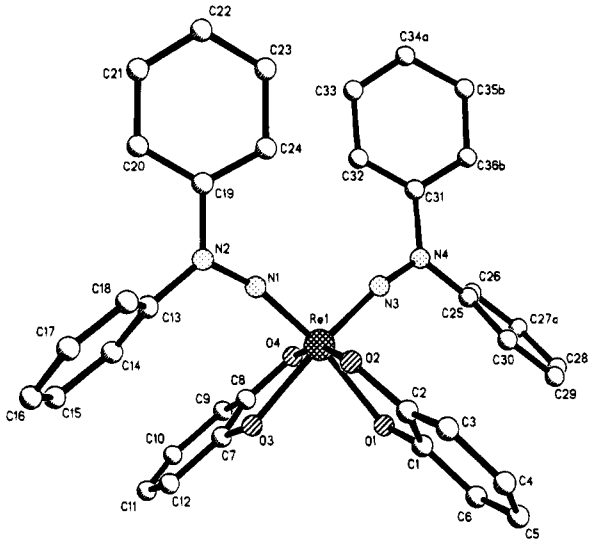

Figure 3. View of the structure of $[Re(NNPh_2)_2(O_2C_6H_4)_2]^{1-}$.

1.20−1.24 Å, respectively, while those for the *cis*-$\{M(NNR_2)_2\}$ cores lay within the 1.77−1.79 and 1.29−1.33 Å ranges, respectively. Whether these characteristic structural features reflect primarily steric or electronic factors of the bonding remains unresolved. The limited data for five-coordinate complexes exhibiting the *cis*-$\{M(NNR)_2\}$ and *cis*-$\{M(NNR_2)_2\}$ cores reveal that in $[TcCl(NNAr)_2(PPh_3)_2]$ the Tc−N bond distance is relative contracted to *ca.* 1.79 Å and, thus, in the range associated with the *cis*-bis(hydrazido) cores, while the N−N bond distance is unaffected. This observation may suggest that the M−N distances associated with the six-coordinate complexes of the $\{M(NNR)_2\}$ core are lengthened as a consequence of steric crowding about the metal site. However, as we have noted previously, the contraction of the N−M−N valence angles in these complexes reflects a potential direct interaction of the N_α groups, a factor which also would tend to lengthen the M−N bond distances. The significantly longer N−N bond distances associated with the *cis*-$\{M(NNR_2)_2\}$ cores may also be primarily steric in origin, simply reflecting the geometric consequences of introducing a second substituent on N_β. The concomitant expansion of the N−M−N in these instances would reinforce this interpretation.

Another noteworthy feature of structures **5** and **8** is the singly-bent organodiazenido units, which serve formally as monocationic, three-electron-donating groups in an analogous fashion to the linear nitrosyl group.[41] Such a formalism would render the Tc oxidation sate +1. In contrast, the diorganohydrazido groups of **7** are unambiguously −2 ligands, giving an oxidation state of +5 for the Re. The strong structural analogies associated with **5**, **7**, and **8** and the Cis-$\{M(NNR)_2\}$ and *cis*-$\{M(NNR_2)_2\}$ cores in general suggest that the effective metal oxidation states for these units are similar. This observation is supported by the ^{99}Tc NMR spectroscopy of $[TcCl(NNAr)_2(PPh_3)_2]$ which exhibits a resonance in the chemical shift region characteristic of Tc(V) not of Tc in the −1 oxidation state. We conclude that, despite the usefulness of the diazenido(1+) formalism, the complexes of this study are more realistically regarded as Re(V) species.

Conclusions

The organohydrazine chemistry of rhenium is quite extensive, and the facile substitution of rhenium oxo groups by organodiazenido and organohydrazido units in rhenium−catecholate species has been established. Since the use of hydrazido-based linkers in the preparation of new technetium complexes for use in diagnostic nuclear medicine has been established, the development of the parallel chemistry of the rhenium congener may prove useful. The observation that oxorhenium(V)−catecholate complexes serve as effective precursors in the uptake of $^{186,188}Re$ by hydrazinopyridine-modified IgG suggested that the formation of the Re−hydrazido functionality is a key step in this process. Since the structure of the metalated complex conjugate is unknown, subsequent deprotonation to form a diazenido species $\{Re(NNR)\}$ rather than the hydrazido form $\{Re(NNHR)\}$, which would be the analogue to the structures of this study, cannot be excluded. While bishydrazido species with the $\{Re(NNR_2)_2\}$ core are the most readily formed, there is no evidence to support or the preclude the binding of two IgG groups to a single metal center in the modified IgG conjugate complex. However, this study does confirm the feasibility of possible reaction pathway, establishes the robust nature of the $\{Re(NNR)_2\}$ unit, and provides simple inorganic models for the labeling chemistry.

Acknowledgment. This work was supported by the U.S. Department of Energy, Grant No. DE-FG02-93ER61571.

Supplementary Material Available: Tables of atomic positional parameters, bond lengths and angles, anisotropic temperature factors, and calculated hydrogen atom positions for **5**, **7**, and **8** (26 pages). Ordering information is given on any current masthead page.